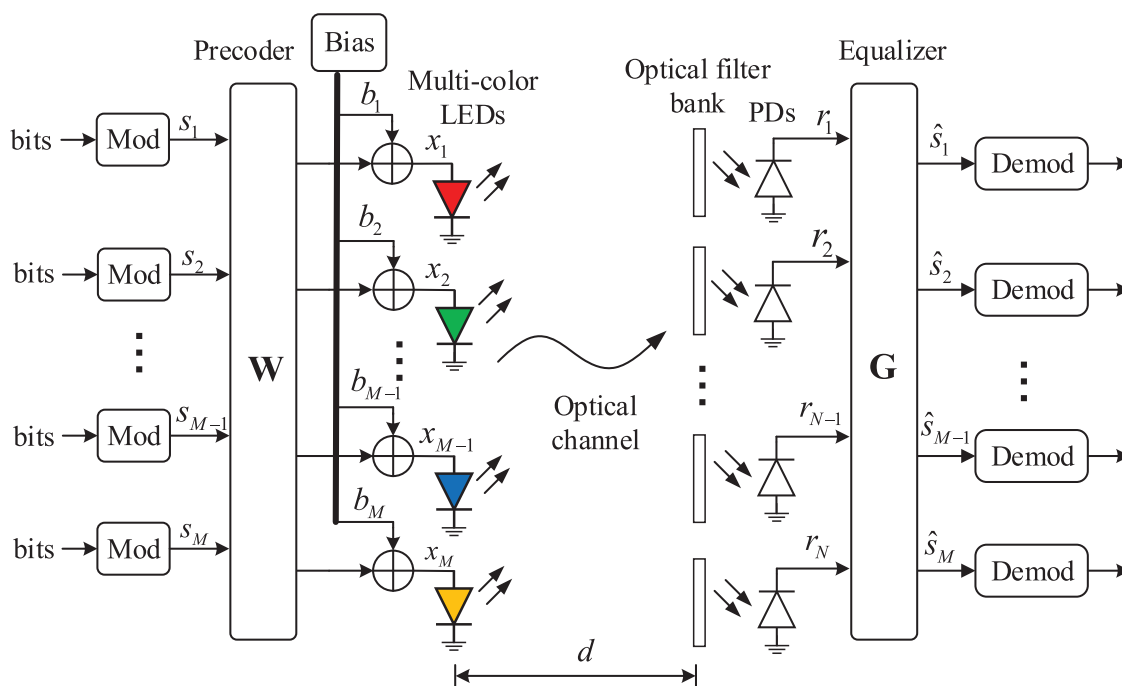


Optical Filter Bank Modeling and Design for Multi-Color Visible Light Communications






Volume 13, Number 1, February 2021

Pengfei Ge
 Xintong Ling, *Member, IEEE*
 Jiaheng Wang, *Senior Member, IEEE*
 Xiao Liang, *Member, IEEE*
 Shuo Li, *Graduate Student Member, IEEE*
 Chunming Zhao, *Member, IEEE*



DOI: 10.1109/JPHOT.2021.3053177

Optical Filter Bank Modeling and Design for Multi-Color Visible Light Communications

Pengfei Ge ¹, Xintong Ling ^{1,2} *Member, IEEE*,
Jiaheng Wang ^{1,2} *Senior Member, IEEE*,
Xiao Liang ^{1,2} *Member, IEEE*,
Shuo Li,¹ *Graduate Student Member, IEEE*,
and Chunming Zhao ^{1,2} *Member, IEEE*

¹National Mobile Communications Research Lab, Southeast University, Nanjing 210096, China

²Purple Mountain Laboratories, Nanjing 211111, China

DOI:10.1109/JPHOT.2021.3053177

This work is licensed under a Creative Commons Attribution 4.0 License. For more information, see <https://creativecommons.org/licenses/by/4.0/>

Manuscript received November 16, 2020; revised January 12, 2021; accepted January 15, 2021. Date of publication January 20, 2021; date of current version February 9, 2021. This work was supported in part by the National Key R&D Program of China under Grant 2018YFB1801103, in part by the National Natural Science Foundation of China under Grants 61901111, 61971130, 61871112, and 61720106003, in part by the Natural Science Foundation of Jiangsu Province under Grant BK20190331, in part by the Jiangsu Province Basic Research Project under Grant BK20192002, in part by the Research Fund of the National Mobile Communications Research Laboratory, Southeast University under Grant 2019B02, in part by Huawei Cooperation Project, and in part by the Fundamental Research Funds for the Central Universities. This paper was presented in part at the IEEE Global Communications Conference 2019 (GLOBECOM 2019), Waikoloa, HI, USA, December 2019 [1]. Corresponding authors: Xintong Ling; Jiaheng Wang (e-mail: xtling@seu.edu.cn; jhwang@seu.edu.cn).

Abstract: Multi-color visible light communication (MC-VLC) can achieve a multi-fold rate by taking advantage of multiple color channels. The optical filters for separating different colors are often designed for the normal incidence case only. However, the center wavelength (CWL) of the optical filter shifts as the angle of incidence (AOI) varies, leading to performance degradation. To address the issue caused by the CWL shift, we propose a novel concept of the optical filter bank that uses a group of narrow-band optical filters and divides the whole visible light spectrum into many narrow bands of wavelengths. The optical filter bank can flexibly combine the useful signal of each monochromatic color and effectively avoid the undesired interference, even if the CWL shifts. Based on the optical filter bank, we establish the channel model and signal model of the MC-VLC system, and then jointly design the linear precoding and equalization for MC-VLC. As illustrated by simulations, the proposed optical filter bank transceiver can achieve a high rate and stable performance at varying AOIs.

Index Terms: Center wavelength (CWL) shift, linear transceiver design, optical filter bank, precoder, visible light communication.

1. Introduction

Visible light communication (VLC) using light-emitting diodes (LEDs) has drawn substantial attention from both academic and industry in recent years [2], [3]. VLC offers the dual functions of communication and illumination simultaneously, referred to as communication-lighting integration [4]. Compared with radio frequency (RF) communication, VLC has attractive characteristics such

as low cost, high security, plenty of license-free bandwidth, and no interference with sensitive electronic equipment (see e.g., [5], [6]). Owing to these advantages, VLC emerges as a promising technology for the next generation of wireless communication [7].

Multi-color VLC (MC-VLC) uses multi-color LEDs, which consist of several LED chips emitting different monochromatic lights, to transmit data in a color division manner [8], [9]. Compared with single-color VLC, MC-VLC can not only provide adjustable illumination in terms of color temperature (CT) and color rendering index (CRI), but also achieve a multi-fold increase in channel capacity [10]. In MC-VLC, optical filters are usually adopted to separate the signals of different colors [11]–[13]. There are two types of optical filters: color-glass optical filters and thin-film optical filters. Between them, thin-film optical filters are widely used, due to the high in-band transmission, deep out-of-band attenuation, and sharp passband edges [14]. Nowadays, the passband bandwidth (BW) and center wavelength (CWL) of the thin-film optical filters can be specifically customized according to the requirement [14].

In the conventional MC-VLC, each individual optical filter is designed for a monochromatic color to balance the trade-off between the useful signals and undesired interferences. In [15], the authors used a multiple-input multiple-output (MIMO) detection method (zero-forcing equalization) to mitigate cross-color interference. The authors in [16] proposed a scheme that recovers the transmit signal by image processing algorithms for camera-based receivers. In [17], the BW and CWL of optical filters were optimized to maximize the signal-to-interference-plus-noise ratio (SINR) of the color channel at normal incidence. The authors in [18] considered the BW and CWL optimization of the optical filters for linear minimum mean square error (LMMSE) receivers at normal incidence. However, in practice, the light is not always incident normally. As the angle of incidence (AOI) increases, the CWL of thin-film optical filter shifts to shorter wavelengths, also known as the “blue shift”. As a result, the passband of the optical filter designed for normal incidence deviates away from its required wavelength range [1], [19]. Consequently, the undesired signals cannot be eliminated effectively and the desired signal attenuates severely, leading to performance degradation. Therefore, it is a critical and challenging issue to deal with the CWL shift caused by varying AOIs.

To address the performance degradation caused by the CWL shift, several optical filter designs were proposed. In [18], a statistically robust and a worst-case robust optical filter designs were proposed to minimize the sum-MSE in the average and worst-case sense, respectively. In [20], the authors proposed an optical filter with the passband out of alignment towards a longer wavelength to compensate for the CWL shift. These existing works [18], [20] adjusted the CWL to a longer wavelength to combat the CWL shift. Such optical filter designs improve the performance at large AOIs, but cause performance degradation at normal incidence and cannot guarantee stable performance for different AOIs.

In this work, to deal with the issue caused by the CWL shift and achieve stable performance for different AOIs, we propose a novel filtering structure named optical filter bank. The optical filter bank uses a group of narrow-band optical filters and covers seamlessly the whole visible light spectrum and divides it into many narrow bands of wavelengths. Compared with the conventional filtering structure, the proposed optical filter bank offers several significant advantages for MC-VLC. First, by dividing the visible light spectrum into multiple narrow bands, the optical filter bank can effectively collect the useful signal power and eliminate the interferences. Second, the optical filter bank is flexible for different AOIs and can combine the desired narrow bands adaptively, even if the CWL shifts with varying AOIs. Third, the optical filter bank has great compatibility for different LEDs with different spectral shapes.

To combine the narrow bands of wavelengths in MC-VLC, the equalization matrix is necessary. Meanwhile, the transmitted signals shall also be properly processed by a precoding matrix. Thus, the transmit precoding and receive equalization are important for MC-VLC using optical filter bank, and thus shall be carefully designed. For this purpose, we establish the system model for the optical-filter-bank-based MC-VLC, and jointly design linear precoding and equalization for optical filter bank transceivers under various constraints. Such a problem is, however, not easy to tackle

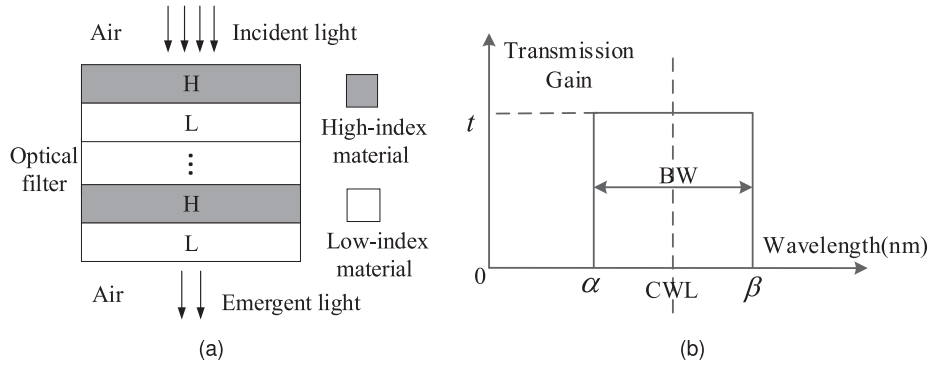


Fig. 1. (a) Internal structure of a thin-film optical filter. (b) Passband shape of a thin-film optical filter.

due to the non-convex objective function and complicated constraints. In this work, our main contributions are summarized in the following:

- We propose the novel concept of optical filter bank for MC-VLC to address the performance degradation caused by the CWL shift.
- We establish the channel model and signal model for MC-VLC using optical filter bank.
- We propose an effective algorithm to jointly design the linear precoding and equalization for MC-VLC transceivers with optical filter bank.
- In the simulations, we show the superiority of the optical filter bank and transceiver design algorithm, even with the varying AOs.

The rest of the paper is organized as follows. In Section 2, we begin with the CWL shift of optical filters. In Section 3, we propose the optical filter bank and establish the channel model and signal model. Section 4 formulates the transceiver design problem for MC-VLC using optical filter bank. Section 5 demonstrates the simulation results. Finally, conclusions are drawn in Section 6.

Notation: Bold uppercase and lowercase letters are used for matrices and vectors, respectively. $(\cdot)^T$ and $(\cdot)^{-1}$ denote the transpose and inverse of a matrix, respectively. $\mathbb{E}[\cdot]$ denotes the expectation. $\text{Tr}(\cdot)$ is the trace of a matrix. The operators \geq and \leq are defined element-wise for vectors. $\min(\cdot)$ denotes an element-wise minimum operator. $\text{abs}(\cdot)$ denotes an element-wise absolute operator. \circ denotes the Hadamard (element-wise) product. \mathbf{I}_M denotes an $M \times M$ identity matrix. $\mathbf{1}_M$ denotes the $M \times 1$ column vector of ones. $\text{diag}(\mathbf{a})$ denotes a diagonal matrix with \mathbf{a} being its diagonal entries. $[\mathbf{A}]_{i,j}$ denotes the i -th row and the j -th column element of matrix \mathbf{A} . $[\mathbf{A}]_{i,:}$ denotes the i -th row vector of matrix \mathbf{A} . $\|\cdot\|_1$ and $\|\cdot\|_2$ denote the l_1 and l_2 norms of a vector, respectively. $\|\cdot\|_F$ denotes the Frobenius norm of a matrix. $\mathbf{A} \succeq \mathbf{0}$ indicates that matrix \mathbf{A} is positive semi-definite.

2. CWL Shift of Optical Filter

Thin-film optical filters, composed of multiple thin dielectric layers, have been widely used in MC-VLC systems to separate different color channels [21]. Fig. 1(a) illustrates the internal structure of a thin-film optical filter, which is made up of alternating layers of high- (H) and low- (L) index materials. As the number of high and low-index layers (in pairs) increases, constructive interference or destructive interference occurs at particular wavelength ranges, leading to the passband or stopband of the optical filter [22].

As illustrated in Fig. 1(b), thin-film optical filters have near-ideal bandpass characteristics, including high in-band transmission, deep out-of-band attenuation, and sharp passband edges [19]. Therefore, the passband of a thin-film optical filter can be considered as rectangular in shape, characterized by three parameters: in-band transmission gain t , BW, and CWL. BW and CWL can be expressed in terms of the left and right passband edges α and β :

$$\text{BW} = \beta - \alpha, \text{CWL} = \frac{\alpha + \beta}{2}. \quad (1)$$

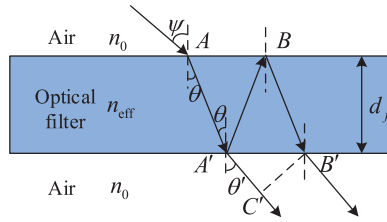


Fig. 2. Phenomenon of light interference of a thin-film optical filter.

Due to the principle of light interference, the CWL of a thin-film optical filter shifts towards shorter wavelengths as the AOI is increased from 0° to large values, also known as the “blue shift” [19]. Let $\lambda_0(\psi)$ be the CWL at an AOI ψ , and define $\lambda_0 = \lambda_0(0)$ as the CWL of the optical filter at normal incidence. From the phenomenon of light interference of a thin-film optical filter illustrated in Fig. 2, we would like to summarize the relationship between $\lambda_0(\psi)$, λ_0 , and the AOI ψ in Lemma 1 as follows.

Lemma 1: [23] The CWL shift of a thin-film optical filter can be characterized as

$$\lambda_0(\psi) = \lambda_0 \cdot \sqrt{1 - \left(\frac{n_0 \sin(\psi)}{n_{\text{eff}}} \right)^2}, \quad (2)$$

where n_0 and n_{eff} are the effective refractive indexes of the air and the optical filter, respectively.

Proof: In Fig. 2, the optical path difference between the adjacent two rays $A'B$ and $A'C'$ is

$$\Delta l = (A'B + BB')n_{\text{eff}} - A'C'n_0. \quad (3)$$

From the geometric relationship in Fig. 2, we can obtain that $A'B = BB' = \frac{d_f}{\cos(\theta)}$, $A'C' = A'B \sin(\theta')$, and $A'B' = 2d_f \tan(\theta)$, where d_f is the thickness of the optical filter. According to the law of refraction, we have $n_{\text{eff}} \sin(\theta) = n_0 \sin(\psi)$ and $n_{\text{eff}} \sin(\theta) = n_0 \sin(\theta')$. Thus, we can express Δl as

$$\Delta l = 2d_f n_{\text{eff}} \sqrt{1 - \left(\frac{n_0 \sin(\psi)}{n_{\text{eff}}} \right)^2}. \quad (4)$$

To generate constructive interference at the CWL $\lambda_0(\psi)$, Δl shall satisfy the condition

$$\frac{2\pi \Delta l}{\lambda_0(\psi)} = 2\pi m, \quad m = 1, 2, \dots \quad (5)$$

By substituting (4) into (5), we have

$$\frac{2d_f n_{\text{eff}} \sqrt{1 - \left(\frac{n_0 \sin(\psi)}{n_{\text{eff}}} \right)^2}}{\lambda_0(\psi)} = m, \quad m = 1, 2, \dots \quad (6)$$

At normal incidence $\psi = 0^\circ$, we can obtain from (6) that

$$\frac{2d_f n_{\text{eff}}}{\lambda_0} = m, \quad m = 1, 2, \dots \quad (7)$$

Combining (6) and (7), we can conclude with Lemma 1. ■

Lemma 1 characterizes the CWL shift with the AOI. From (2), one can find that $\lambda_0(\psi)$ is decreasing in ψ , implying that CWL shifts towards shorter wavelength as the AOI increases. The CWL shift is not only affected by the AOI, but also the effective refractive indexes of the air and the optical filter, i.e., n_0 and n_{eff} . According to (2), $\lambda_0(\psi)$ is increasing in n_{eff} , implying that the smaller n_{eff} is, the more significant the CWL shift is. Denote $(\alpha(\psi), \beta(\psi))$ as the passband edge pair at an AOI ψ . Similarly, the relationship between $(\alpha(\psi), \beta(\psi))$ and $(\alpha(0), \beta(0))$ can also be characterized by Lemma 1.

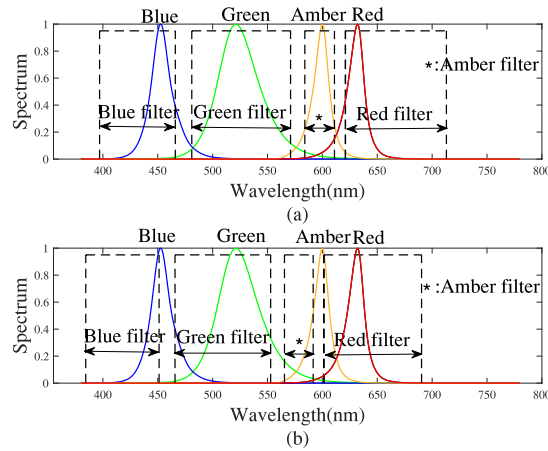


Fig. 3. Conventional optical filter design at normal incidence and the spectra of RGBA LEDs. (a) $\psi = 0^\circ$. (b) $\psi = 30^\circ$.

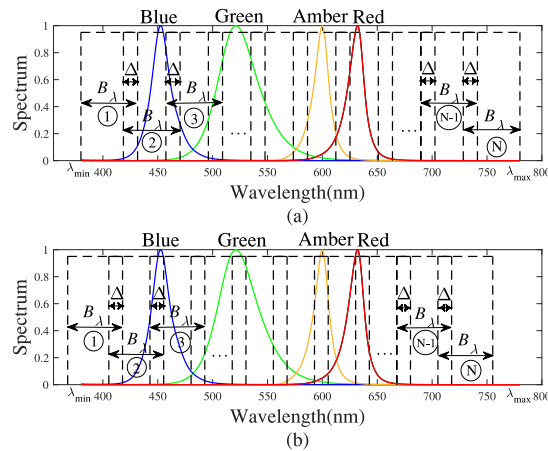


Fig. 4. Proposed optical filter bank ($N = 10$ and $\gamma = 0.25$) and the spectra of RGBA LEDs. (a) $\psi = 0^\circ$. (b) $\psi = 30^\circ$.

Conventional MC-VLC systems adopt the filtering structure that each individual optical filter corresponds to a color channel. Fig. 3 presents a conventional optical filter design and the spectra of red/green/blue/amber (RGBA) monochromatic LEDs in an MC-VLC system. The passband of every optical filter is designed for a single color channel to maximize the SINR at normal incidence [17]. From Fig. 3(a), signals of different monochromatic spectra are separated well at normal incidence ($\psi = 0^\circ$). However, in Fig. 3(b), the filter CWLs shift towards a shorter wavelength at $\psi = 30^\circ$, and the desired color signals attenuate severely and the undesired signals cannot be eliminated effectively. As the AOI deviates from the normal, the filter passband of each color channel shifts away from its desired wavelength range, leading to degraded performance.

3. MC-VLC Using Optical Filter Bank

3.1 Optical Filter Bank

To combat the issue caused by the CWL shift, we propose a novel filtering structure named optical filter bank for MC-VLC, as illustrated in Fig. 4. In the optical filter bank, the number of optical filters N is larger than the number of monochromatic LEDs M . These optical filters has narrow,

identical passband BW, denoted by B_λ . The passbands of adjacent optical filters overlap with a ratio $\gamma \in [0, 1)$, defined as

$$\gamma = \frac{\Delta}{B_\lambda}, \quad (8)$$

where $\Delta \in [0, B_\lambda)$ is the overlapped bandwidth. Apparently, the optical filter bank covers the whole visible spectrum between λ_{\min} and λ_{\max} . Given the number of optical filters N , the BW of an optical filter is

$$B_\lambda = \frac{\lambda_{\max} - \lambda_{\min}}{N - N\gamma + \gamma}. \quad (9)$$

Hence, the number of optical filters N and the passband overlap ratio γ determine the left and right passband edges of the i -th optical filter:

$$\alpha_i = \lambda_{\min} + (i - i\gamma + \gamma - 1)B_\lambda, \quad (10)$$

$$\beta_i = \lambda_{\min} + (i - i\gamma + \gamma)B_\lambda. \quad (11)$$

In Fig. 4, the optical filter bank with $N = 10$ and $\gamma = 0.25$ is presented as an example. One can see that the whole visible light spectrum is seamlessly covered and is divided into many narrow bands of wavelengths. Such a filtering structure offers several advantages for MC-VLC in comparison with that in Fig. 3. First, the optical filter bank provides effective SINR for each color channel, since it can avoid undesired interference by using narrow-band optical filters and guarantee enough useful signal power by using more optical filters. Second, the optical filter bank can adaptively combine the desired narrow bands of wavelengths and avoid the undesired ones, resulting in flexibility for different AOs. Third, the optical filter bank is compatible for different configurations of LEDs, since the spectra with different shapes can be recovered by combining the narrow bands of wavelengths.

Remark 1: According to (9), the BW B_λ is decreasing and increasing in the optical filter number N and the passband overlap ratio γ , respectively. This implies that N and γ have a great impact on the optical filter bank. A small N leads to a broad B_λ , making the cross-color interference in each optical filter more serious; A large N leads to a rather narrow B_λ , making the received optical signal of each optical filter weaker and the channel noise dominant. Thus, N should not be too large or small. For the same reason, γ should not be too large or small, either. The effect of N and γ will be discussed in Section 5.3.

3.2 Channel Model of Optical Filter Bank

In this subsection, we would like to establish the channel model for MC-VLC using optical filter bank. Consider an MC-VLC system equipped with optical filter bank in Fig. 5. Let $S_j(\lambda)$ be the spectral shape of the j -th LED. Generally, $S_j(\lambda)$ can be described by the H model as [24]

$$S_j(\lambda) = \frac{g(\lambda, \lambda_j, \Delta\lambda_j) + k_{j,1} \cdot g^{k_{j,2}}(\lambda, \lambda_j, \Delta\lambda_j)}{1 + k_{j,1}}, \quad (12)$$

with

$$g(\lambda, \lambda_j, \Delta\lambda_j) = \exp\left[-\frac{(\lambda - \lambda_j)^2}{\Delta\lambda_j^2}\right], \quad (13)$$

$$\Delta\lambda_j = \begin{cases} \Delta\lambda_{j,1}, & \lambda < \lambda_j \\ \Delta\lambda_{j,2}, & \lambda \geq \lambda_j, \end{cases} \quad (14)$$

where λ_j is the peak wavelength of the spectrum, $\Delta\lambda_{j,1}$ is the left half-spectral width satisfying $S_j(\lambda_j - \Delta\lambda_{j,1}) = \frac{1}{2}S_j(\lambda_j)$, $\Delta\lambda_{j,2}$ is the right half-spectral width satisfying $S_j(\lambda_j + \Delta\lambda_{j,2}) = \frac{1}{2}S_j(\lambda_j)$, and $k_{j,1} \in \mathbb{N}$ and $k_{j,2} \in \mathbb{N}$ represent the characteristic parameters of the spectral shape.

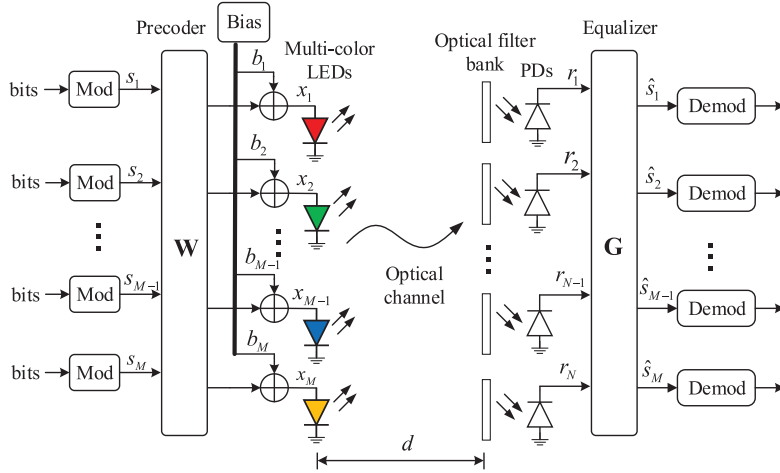


Fig. 5. System model of MC-VLC equipped with optical filter bank.

Let ϕ be the angle of irradiance of the transmitter, ψ be the angle of incidence of the receiver, and d be the distance between the transmitter and the receiver. Since the physical sizes of both the multi-color LED cluster and the photodiode (PD) cluster are much smaller than the distance d , they can be regarded as points so that the subchannels between different monochromatic LEDs and PDs have the identical d , ψ , and ϕ . Thus, the gain of the MC-VLC link can be written as

$$h_{dc} = \begin{cases} \frac{L(\phi)AR_0 \cos(\psi)}{d^2}, & 0 \leq \psi \leq \Psi_m \\ 0, & \psi > \Psi_m, \end{cases} \quad (15)$$

where A is the area of each PD, R_0 is the responsivity¹ of PD, and Ψ_m is the field of view (FoV) of the receiver. Besides, $L(\phi)$ is the radiant pattern of the light emitting, which can be described by a Lambertian model as [28]:

$$L(\phi) = \frac{m+1}{2\pi} \cos^m \phi, \quad (16)$$

where m is the Lambertian emission order related to the half-power semi-angle $\Phi_{1/2}$ by $m = -\ln 2 / \ln(\cos \Phi_{1/2})$.

Taking the spectral shape of the LED into consideration, we can express the gain of subchannel from the j -th monochromatic LED to the i -th PD as

$$h_{ij} = h_{dc} \frac{\eta_j \int_{\alpha_i(\psi)}^{\beta_i(\psi)} S_j(\lambda) d\lambda}{\int_{-\infty}^{+\infty} S_j(\lambda) d\lambda}, \quad (17)$$

where $\alpha_i(\psi)$ and $\beta_i(\psi)$ are the passband edges of the i -th optical filter at an AOI ψ , respectively, and η_j is the electro-optic (E-O) conversion factor of the j -th monochromatic LED.

Therefore, the MIMO channel model for the MC-VLC using optical filter bank can be written as

$$\mathbf{H} = (h_{ij})^{N \times M}. \quad (18)$$

The channel matrix \mathbf{H} in (18) is highly related to the filter passband edges $\alpha_i(\psi)$ and $\beta_i(\psi)$ for $i = 1, 2, \dots, N$. Since $\alpha_i(\psi)$ and $\beta_i(\psi)$ for $i = 1, 2, \dots, N$ vary with the AOI as described in Lemma 1, one can find that the channel matrix \mathbf{H} is heavily influenced by the AOI.

¹In this work, we use the assumption that the responsivity of a PD is approximately constant in the visible light spectrum [25]–[27]. In the case that the responsivity changes with the wavelength, our proposed structure is still available since the impact of the responsivity has been included in the channel matrix \mathbf{H} .

The conventional filtering structure in Fig. 3 generates parallel color channels by directly separating different monochromatic spectra. Unlike the conventional one, the proposed optical filter bank uses a group of narrow-band optical filters to divide the whole visible light spectrum into many narrow bands of wavelengths. As a result, to generate parallel color channels, the narrow bands of wavelengths shall be adaptively combined by an equalization matrix. Besides, the transmitted signals shall also be properly processed by a precoding matrix. In the following, we will jointly design the linear precoding and equalization for MC-VLC transceiver using optical filter bank.

3.3 Signal Model

The MC-VLC using the optical filter bank with the optical filter number N and passband overlap ratio γ is illustrated in Fig. 5. There are M independent substreams, and the symbol of the k -th substream is $s_k \in [-1, 1]$ with $\mathbb{E}[s_k] = 0$ and $\mathbb{E}[s_k^2] = \sigma_s^2$. The symbol vector can be written as $\mathbf{s} = [s_1, \dots, s_M]^T$ with the covariance matrix $\mathbf{R}_s = \mathbb{E}[\mathbf{s}\mathbf{s}^T] = \sigma_s^2 \mathbf{I}_M$. \mathbf{s} is first precoded by a matrix $\mathbf{W} \in \mathbb{R}^{M \times M}$, and then added with a direct current (DC) bias vector $\mathbf{b} \in \mathbb{R}^{M \times 1}$ to generate the non-negative signals

$$\mathbf{x} = \mathbf{W}\mathbf{s} + \mathbf{b}. \quad (19)$$

The lights of multi-color LEDs mix and radiate for the functions of illumination and communication.

At the receiver, the modulated light is captured by the optical filter bank and converted into the electrical signal, written as

$$\mathbf{r} = \mathbf{H}\mathbf{x} + \mathbf{n} = \mathbf{H}\mathbf{W}\mathbf{s} + \mathbf{H}\mathbf{b} + \mathbf{n}, \quad (20)$$

where \mathbf{H} is the MIMO channel matrix in (18), and \mathbf{n} is the receiver noise vector obeying a zero-mean Gaussian distribution, i.e., $\mathbf{n} \sim \mathcal{N}(\mathbf{0}, \mathbf{R}_n)$.

After removing the DC component $\mathbf{H}\mathbf{b}$ in (20), we have the signal vector

$$\mathbf{y} = \mathbf{H}\mathbf{W}\mathbf{s} + \mathbf{n}. \quad (21)$$

The symbol vector \mathbf{s} is recovered by equalizing \mathbf{y} via multiplying a matrix $\mathbf{G} \in \mathbb{R}^{M \times N}$, each row of which acts as a weight vector to combine the narrow ranges of wavelengths for a color channel. The estimated symbol vector $\hat{\mathbf{s}}$ is expressed as

$$\hat{\mathbf{s}} = \mathbf{G}\mathbf{y}. \quad (22)$$

Therefore, due to the CWL shift with varying AOIs, the precoding matrix \mathbf{W} and equalization matrix \mathbf{G} shall be carefully designed for MC-VLC systems using optical filter bank.

4. Linear Transceiver Design for Optical Filter Bank

4.1 Problem Formulation

We use the sum-MSE of all the M substreams as a criterion to assess the system performance [29]–[34]. The covariance matrix of the MSE of the M substreams is given by

$$\begin{aligned} \mathbf{R}_e &= \mathbb{E}[(\hat{\mathbf{s}} - \mathbf{s})(\hat{\mathbf{s}} - \mathbf{s})^T] = \mathbb{E}\{[\mathbf{G}(\mathbf{H}\mathbf{W}\mathbf{s} + \mathbf{n}) - \mathbf{s}][\mathbf{G}(\mathbf{H}\mathbf{W}\mathbf{s} + \mathbf{n}) - \mathbf{s}]^T\} \\ &= \mathbf{G}\mathbf{H}\mathbf{W}\mathbf{R}_s\mathbf{W}^T\mathbf{H}^T\mathbf{G}^T + \mathbf{R}_s + \mathbf{G}\mathbf{R}_n\mathbf{G}^T - 2\mathbf{G}\mathbf{H}\mathbf{W}\mathbf{R}_s. \end{aligned} \quad (23)$$

Thus, the sum-MSE can be written as

$$\text{MSE}(\mathbf{W}, \mathbf{G}) = \text{Tr}(\mathbf{R}_e) = \text{Tr}(\mathbf{G}\mathbf{H}\mathbf{W}\mathbf{R}_s\mathbf{W}^T\mathbf{H}^T\mathbf{G}^T + \mathbf{R}_s + \mathbf{G}\mathbf{R}_n\mathbf{G}^T - 2\mathbf{G}\mathbf{H}\mathbf{W}\mathbf{R}_s). \quad (24)$$

In the design of precoder \mathbf{W} and equalizer \mathbf{G} , several constraints shall be considered.

1) Limited dynamic range constraint: The LED is dynamic-range limited. For the j -th LED, the driving signal is bounded by a turn-on value $x_{\text{on},j}$ and a saturation value $x_{\text{sat},j}$, and thus the driving signal vector of multi-color LEDs $\mathbf{W}\mathbf{s} + \mathbf{b}$ shall satisfy

$$\mathbf{W}\mathbf{s} + \mathbf{b} \geq \mathbf{x}_{\text{on}}, \quad (25)$$

$$\mathbf{W}\mathbf{s} + \mathbf{b} \leq \mathbf{x}_{\text{sat}}, \quad (26)$$

where $\mathbf{x}_{\text{on}} = [x_{\text{on},1}, \dots, x_{\text{on},M}]^T$ and $\mathbf{x}_{\text{sat}} = [x_{\text{sat},1}, \dots, x_{\text{sat},M}]^T$.

2) Color illumination constraint: To mix the multi-color lights into the white light with a target CT and CRI, the average optical powers of the multi-color lights shall satisfy a pre-determined color mixture ratio (CMR) $\mathbf{c} = [c_1, \dots, c_M]$ (\mathbf{c} is normalized as $\sum_{k=1}^M c_k = 1$) [35], i.e.,

$$\mathbb{E}[\boldsymbol{\eta} \circ (\mathbf{W}\mathbf{s} + \mathbf{b})] = \boldsymbol{\eta} \circ \mathbf{W}\mathbb{E}[\mathbf{s}] + \boldsymbol{\eta} \circ \mathbf{b} = \boldsymbol{\eta} \circ \mathbf{b} = \boldsymbol{\xi} \mathbf{c}, \quad (27)$$

where $\boldsymbol{\eta} = [\eta_1, \dots, \eta_M]^T$ is the vector of E-O conversion factors of LEDs, and $\boldsymbol{\xi}$ is a certain scalar.

3) Total brightness level constraint: The mixed multi-color lights shall provide a target total brightness level L_T , and thus we have

$$\mathbb{E}[\boldsymbol{\eta}^T (\mathbf{W}\mathbf{s} + \mathbf{b})] = \boldsymbol{\eta}^T \mathbf{W}\mathbb{E}[\mathbf{s}] + \boldsymbol{\eta}^T \mathbf{b} = \boldsymbol{\eta}^T \mathbf{b} = L_T. \quad (28)$$

Therefore, the transceiver design problem in MC-VLC to minimize the sum-MSE under the above constraints can be formulated as

$$\min_{\mathbf{W}, \mathbf{G}} \text{MSE}(\mathbf{W}, \mathbf{G}) \quad (29a)$$

$$\text{s.t. } \mathbf{W}\mathbf{s} + \mathbf{b} \geq \mathbf{x}_{\text{on}} \quad (29b)$$

$$\mathbf{W}\mathbf{s} + \mathbf{b} \leq \mathbf{x}_{\text{sat}} \quad (29c)$$

$$\boldsymbol{\eta} \circ \mathbf{b} = \boldsymbol{\xi} \mathbf{c} \quad (29d)$$

$$\boldsymbol{\eta}^T \mathbf{b} = L_T. \quad (29e)$$

Such a transceiver design problem in MC-VLC has a similar form as that in MIMO VLC systems [29]–[34]. Generally, the transceiver design problem in VLC is difficult to deal with due to the complicated objective function $\text{MSE}(\mathbf{W}, \mathbf{G})$ with respect to \mathbf{W} and \mathbf{G} in (24), and the constraints in terms of signal amplitude in (25) and (26). In the literature, researchers have been devoted to the study of transceiver design in MIMO VLC systems, and several algorithms have been proposed. In [29], the authors proposed an algorithm that optimizes \mathbf{W} and \mathbf{G} alternatively. In [30], an iterative algorithm based on gradient projection is proposed. The performances of [29] and [30] depend on the initial points. Two problems arise with these existing algorithms. 1) The algorithms in [29] and [30] may converge to bad local optima, when improper initial points are used; 2) Searching many initial points suffers from high computational complexity, and is impractical for MC-VLC with rapidly varying AOIs. Therefore, an algorithm for stable performance with low complexity is urgent.

4.2 Optimal Receiver Design

We first optimize the equalization matrix \mathbf{G} for combining the narrow ranges of wavelengths. Observe that the constraints (29b)–(29e) are unrelated to the equalization matrix \mathbf{G} . Thus, \mathbf{G} can be optimized directly via

$$\frac{\partial \text{MSE}(\mathbf{W}, \mathbf{G})}{\partial \mathbf{G}} = 2\mathbf{G}(\mathbf{H}\mathbf{W}\mathbf{R}_s\mathbf{W}^T\mathbf{H}^T + \mathbf{R}_n) - 2\mathbf{R}_s^T\mathbf{W}^T\mathbf{H}^T = 0. \quad (30)$$

By solving the equation $\frac{\partial \text{MSE}(\mathbf{W}, \mathbf{G})}{\partial \mathbf{G}} = 0$, the optimal \mathbf{G} can be obtained as

$$\mathbf{G}^* = \mathbf{R}_s^T\mathbf{W}^T\mathbf{H}^T(\mathbf{H}\mathbf{W}\mathbf{R}_s\mathbf{W}^T\mathbf{H}^T + \mathbf{R}_n)^{-1}. \quad (31)$$

Such an equalization matrix \mathbf{G}^* is a function with respect to the precoding matrix \mathbf{W} , and play a key role in combining the narrow ranges of wavelengths as the CWL shifts with varying AOIs.

4.3 Transmit Precoder Design

Now we consider the precoding matrix \mathbf{W} . By substituting the obtained optimal \mathbf{G}^* into (24), we have

$$\text{MSE}(\mathbf{W}) = (M - N)\sigma_s^2 + \sigma_s^2 \text{Tr}((\sigma_s^2 \mathbf{H}\mathbf{W}\mathbf{W}^T \mathbf{H}^T + \mathbf{R}_n)^{-1} \mathbf{R}_n). \quad (32)$$

To get rid of the dependence on specific symbol vector \mathbf{s} , the constraints (29b) and (29c) can be rewritten by

$$\text{abs}(\mathbf{W})\mathbf{1}_M \leq \min\{\mathbf{b} - \mathbf{x}_{\text{on}}, \mathbf{x}_{\text{sat}} - \mathbf{b}\}. \quad (33)$$

According to the constraints (29d) and (29e), we can obtain $\xi = L_T$ and $b_j = \frac{L_T c_j}{\eta_j}$. Thus, the constraints in (29b)–(29e) are reduced to a single constraint as

$$\|[\mathbf{W}]_{j,:}\|_1 \leq \min \left\{ \frac{L_T c_j}{\eta_j} - x_{\text{on},j}, x_{\text{sat},j} - \frac{L_T c_j}{\eta_j} \right\}. \quad (34)$$

Therefore, the optimization problem for precoding matrix \mathbf{W} can be expressed as

$$\min_{\mathbf{W}} \text{MSE}(\mathbf{W}) \quad (35a)$$

$$\text{s.t.} \quad \|[\mathbf{W}]_{j,:}\|_1 \leq \min \left\{ \frac{L_T c_j}{\eta_j} - x_{\text{on},j}, x_{\text{sat},j} - \frac{L_T c_j}{\eta_j} \right\}. \quad (35b)$$

Unfortunately, the objective function $\text{MSE}(\mathbf{W})$ in (35a) is non-convex in \mathbf{W} . Due to the constraint in terms of signal amplitude of each LED, the constraint in (35b) is the l_1 norm constraint of each row of \mathbf{W} . As shown by existing works, such a constraint is difficult to deal with, especially along with the non-convex objective function $\text{MSE}(\mathbf{W})$. Thus, it is hard to find the global optimum of problem (35).

To solve problem (35), we introduce a new positive semi-definite matrix $\mathbf{Q} = \mathbf{W}\mathbf{W}^T$. Hence, the objective function can be expressed as

$$\text{MSE}(\mathbf{Q}) = (M - N)\sigma_s^2 + \sigma_s^2 \text{Tr}((\sigma_s^2 \mathbf{H}\mathbf{Q}\mathbf{H}^T + \mathbf{R}_n)^{-1} \mathbf{R}_n). \quad (36)$$

By using the inequality $\|[\mathbf{W}]_{j,:}\|_1 \leq \sqrt{M}\|[\mathbf{W}]_{j,:}\|_2$ [36], the constraints in (35b) is restricted by

$$M[\mathbf{Q}]_{j,j} \leq \min \left\{ \left(\frac{L_T c_j}{\eta_j} - x_{\text{on},j} \right)^2, \left(x_{\text{sat},j} - \frac{L_T c_j}{\eta_j} \right)^2 \right\}. \quad (37)$$

Thus, the problem that optimizes \mathbf{Q} yields an upper bound to the original problem (35)

$$\min_{\mathbf{Q}} \text{Tr}((\sigma_s^2 \mathbf{H}\mathbf{Q}\mathbf{H}^T + \mathbf{R}_n)^{-1} \mathbf{R}_n) \quad (38a)$$

$$\text{s.t.} \quad M[\mathbf{Q}]_{j,j} \leq \min \left\{ \left(\frac{L_T c_j}{\eta_j} - x_{\text{on},j} \right)^2, \left(x_{\text{sat},j} - \frac{L_T c_j}{\eta_j} \right)^2 \right\} \quad (38b)$$

$$\mathbf{Q} \succeq \mathbf{0}. \quad (38c)$$

Obviously, the tightness of this bound depends on the inequality $\|[\mathbf{W}]_{j,:}\|_1 \leq \sqrt{M}\|[\mathbf{W}]_{j,:}\|_2$, which is inversely proportional to M [37]. In MC-VLC, the number of colors M is usually 3 for RGB system or 4 for RGBA system, which are rather small. Thus, it is reasonable to use such inequality in the transceiver design of MC-VLC system.

Now, we characterize problem (38) via Theorem 1.

Theorem 1: By introducing an auxiliary matrix variable $\mathbf{T} \in \mathbb{R}^{N \times N}$, problem (38) can be reformulated as a semi-definite programming (SDP):

$$\min_{\mathbf{Q}, \mathbf{T}} \text{Tr}(\mathbf{T}\mathbf{R}_n) \quad (39a)$$

$$\text{s.t.} \quad M[\mathbf{Q}]_{j,j} \leq \min \left\{ \left(\frac{L_T c_j}{\eta_j} - x_{\text{on},j} \right)^2, \left(x_{\text{sat},j} - \frac{L_T c_j}{\eta_j} \right)^2 \right\} \quad (39b)$$

$$\mathbf{Q} \succeq \mathbf{0} \quad (39c)$$

$$\begin{bmatrix} \mathbf{T} & \mathbf{I} \\ \mathbf{I} & \sigma_s^2 \mathbf{H} \mathbf{Q} \mathbf{H}^T + \mathbf{R}_n \end{bmatrix} \succeq \mathbf{0}. \quad (39d)$$

Proof: Please see the Appendix. ■

The SDP formulation in Theorem 1 makes it possible to find the globally optimal \mathbf{Q}^* by using interior point method [38]. Thus, once the globally optimal \mathbf{Q}^* is obtained, we can obtain the precoding matrix $\hat{\mathbf{W}}$ by decomposing \mathbf{Q}^* as

$$\mathbf{Q}^* = \hat{\mathbf{W}} \hat{\mathbf{W}}^T. \quad (40)$$

The decomposition in (40) can be implemented by Cholesky decomposition (CD) or eigenvalue decomposition (EVD) [36], leading to different precoding matrices $\hat{\mathbf{W}}$'s.

- CD: $\mathbf{Q}^* = \mathbf{L} \mathbf{L}^T$, where \mathbf{L} is a lower triangular matrix, and thus we have $\hat{\mathbf{W}} = \mathbf{L}$.
- EVD: $\mathbf{Q}^* = \mathbf{U} \mathbf{S} \mathbf{U}^T$, where \mathbf{U} is a unitary matrix, and \mathbf{S} is a diagonal matrix with the diagonal elements being the eigenvalues of \mathbf{Q}^* , and thus we have $\hat{\mathbf{W}} = \mathbf{U} \mathbf{S}^{\frac{1}{2}}$.

Though CD and EVD lead to different $\hat{\mathbf{W}}$'s, they have the same objective function sum-MSE.

The precoding matrix $\hat{\mathbf{W}}$ obtained via problem (38) is the upper bound solution to the original problem (35), because the original constraint (35b) is replaced by a stronger one in (38b). Thus, $\hat{\mathbf{W}}$ obtained via problem (38) can be guaranteed to satisfy the original constraint (35b), but (35b) may be inactive. Motivated by this, we can further optimize the objective function sum-MSE by properly scaling $\hat{\mathbf{W}}$ within (35b).

Theorem 2: Define a diagonal matrix

$$\mathbf{\Lambda} = \text{diag}^{-1}(\text{abs}(\hat{\mathbf{W}}) \mathbf{1}_M) \text{diag}(\min\{L_T \text{diag}^{-1}(\boldsymbol{\eta}) \mathbf{c} - \mathbf{x}_{\text{on}}, \mathbf{x}_{\text{sat}} - L_T \text{diag}^{-1}(\boldsymbol{\eta}) \mathbf{c}\}). \quad (41)$$

Let $\xi_{\min}(\mathbf{\Lambda})$ be the minimum value of the diagonal elements of $\mathbf{\Lambda}$. Then, we can further reduce the sum-MSE of problem (35) by

$$\mathbf{W}^* = \xi_{\min}(\mathbf{\Lambda}) \hat{\mathbf{W}}. \quad (42)$$

Proof: By the definition of diagonal matrix $\mathbf{\Lambda}$ in (41), $[\mathbf{\Lambda}]_{j,j} > 1$, and it is the value that scales $[\hat{\mathbf{W}}]_{j,:}$ to activate the dynamic-range constraint of the j -th LED. Thus, $\xi_{\min}(\mathbf{\Lambda})$ is the minimum value that scales $\hat{\mathbf{W}}$ and keeps all the row of the scaled result still within the constraints (35b). Meanwhile, since $\xi_{\min}(\mathbf{\Lambda}) > 1$, the scaling operation in (42) enlarges the transmit signals, and thus we have $\text{MSE}(\mathbf{W}^*) < \text{MSE}(\hat{\mathbf{W}})$. ■

Remark 2: Theorem 2 makes the upper bound of problem (35) tighter. By using the scaling operation in Theorem 2, we can make full use of the original constraint (35b), and improve the performance. More benefits can be found in Section 5.3.

Remark 3: The $\hat{\mathbf{W}}$'s obtained from CD and EVD are different but share the same sum-MSE, since they are decomposed from the same \mathbf{Q}^* . However, after scaling, the sum-MSE of them may be different, since different $\hat{\mathbf{W}}$'s may have different scaling factors $\xi_{\min}(\mathbf{\Lambda})$'s. The performance of CD-scaling and EVD-scaling is compared in Section 5.3.

The proposed transceiver design algorithm that optimizes \mathbf{W} and \mathbf{G} is summarized in Algorithm 1. Unlike the algorithms in [29] and [30], the proposed algorithm does not rely on any initial points. Hence, it can avoid the risk of bad local optimum solutions induced by improper initial points, and can also avoid searching a lot of initial points and thus highly reduce the computational complexity. The proposed algorithm is based on the optimization of an upper bound of (29), and thus the worst-case performance can be guaranteed.

4.4 Complexity of Transceiver Design Algorithm

Now we discuss the complexity of the transceiver design algorithms. The proposed algorithm first solves an SDP problem and then carries out CD or EVD. The complexity is dominated by the solution of the SDP problem via interior point method with the complexity $O(M^{6.5} \log(1/\varepsilon))$, where $\varepsilon > 0$ is the solution accuracy [39]. Thus, the overall complexity is $O(M^{6.5} \log(1/\varepsilon))$.

Algorithm 1: Proposed Transceiver Design Algorithm.

- 1: Input: \mathbf{H} , \mathbf{c} , L_T , \mathbf{x}_{on} , \mathbf{x}_{sat} , η , σ_s^2 , and \mathbf{R}_n .
- 2: Solve the SDP problem in (39) via interior point method, and obtain \mathbf{Q}^* .
- 3: Decompose $\mathbf{Q}^* = \hat{\mathbf{W}}\hat{\mathbf{W}}^T$ by CD or EVD to obtain $\hat{\mathbf{W}}$.
- 4: With the given $\hat{\mathbf{W}}$, obtain \mathbf{W}^* by (42).
- 5: With the given \mathbf{W}^* , obtain \mathbf{G}^* by (31).
- 6: Output: precoding matrix \mathbf{W}^* and equalization matrix \mathbf{G}^* .

The algorithm in [29] optimizes one of \mathbf{W} or \mathbf{G} iteratively while fixing the other. The main complexity results from optimizing \mathbf{W} with fixed \mathbf{G} , which is a linearly constrained quadratic program (LCQP) problem. The LCQP problem can be solved via interior point method with the complexity $O(M^{6.5}\log(1/\varepsilon))$. The algorithm takes n_{ite} iterations to converge, and thus the overall complexity is $O(n_{\text{ite}}M^{6.5}\log(1/\varepsilon))$.

The algorithm in [30] optimizes \mathbf{W} iteratively via gradient projection method. The main complexity results from the projection operation, which has the complexity of $O(M^4)$ [33]. The algorithm takes n_{ite} iterations to converge, and thus the overall complexity is $O(n_{\text{ite}}M^4)$.

Generally, M is 3 or 4 in MC-VLC, the solution accuracy ε of interior point is 10^{-3} , and the number of iteration for the algorithms in [29] and [30] is $n_{\text{ite}} = 50$. Thus, the proposed algorithm has much lower complexity than that in [29], and has comparable complexity with that in [30]. Furthermore, when L initial points are carried out to find a better solution, the complexity of the algorithms in [29] and [30] shall be multiplied with L , leading to even higher complexity. While the proposed algorithm does not depend on the initial points, and retain low complexity.

4.5 Complexity of Optical Filter Bank

Furthermore, we would like to discuss the practical implementation of the proposed optical filter bank structure. In the proposed scheme, we use more optical filters to combat the center wavelength shift. The main problem is that the physical size of hardware increases due to the large number of optical filters. However, as shown in the simulation in Section 5.3, the proposed scheme achieves its best performance when the number $N = 10 \sim 20$. Such an increase is not too much and is acceptable for the implementation. Moreover, as pointed in [40], VLC is developing towards miniaturization with high level of integration, and the area of a PD can be only 0.01 mm^2 . Thus, our proposed optical filter bank scheme is feasible in the practical implementation, especially with the development of modules miniaturization of VLC.

5. Simulation Results

5.1 System Setup

In this section, we evaluate the performance of the optical filter bank via simulations. The commercial quadrichromatic LED (QLED) LZ4-00MA00 (LED Engin) with RGBA LEDs is employed in the system [19]. Fig. 6 illustrates the measured spectra of monochromatic LEDs and H model of LED spectral shape in (12). One can see that the H model can accurately characterize the LED spectrum.

Consider a typical scenario in Fig. 7 where the LEDs and the PDs are vertically downward and upward, respectively. The vertical distance from the transmitter to the receiver is $d_h = 2 \text{ m}$. The CMR for the RGBA color LEDs is $c_1 : c_2 : c_3 : c_4 = 0.14 : 0.45 : 0.11 : 0.30$, which leads to the CT $T_c = 5000 \text{ K}$ and the CIR $R_a = 82$ [35]. The source symbol variance is set to $\sigma_s^2 = 0.42$ by assuming an 8-PAM modulation with zero-mean and bounded within $[-1, 1]$. All the simulation parameters are summarized in Table 1.

Unless stated otherwise, the precoding matrix \mathbf{W} and equalization matrix \mathbf{G} in the simulations are obtained by the proposed algorithm based on CD-scaling.

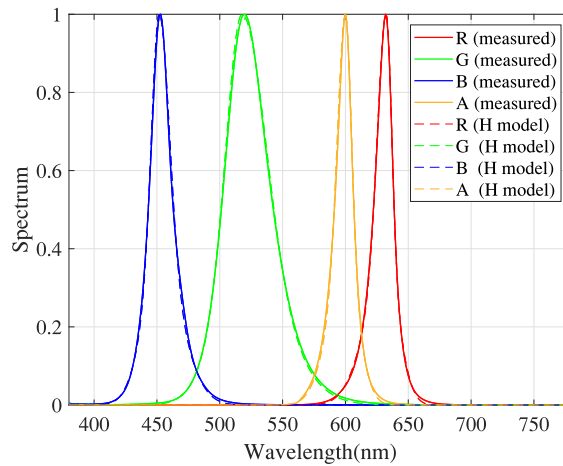


Fig. 6. Measured spectra of RGBA LEDs and H model.

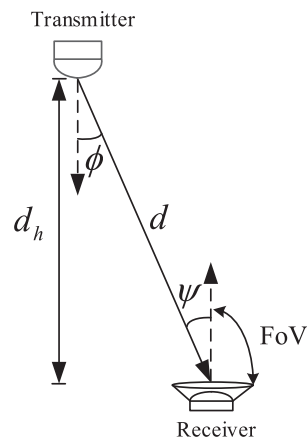


Fig. 7. Geometry of the transmitter and the receiver.

TABLE 1
Simulation Parameters

Parameters	Symbols	Values
The source symbol variance	σ_s^2	0.42
The E-O conversion factor of LEDs	η	[200, 136, 276, 61] lm/A
The min driving signals of LEDs	\mathbf{x}_l	[0, 0, 0, 0] A
The max driving signals of LEDs	\mathbf{x}_u	[1, 1, 1, 1] A
The brightness level	L_T	350 lm
The half power semi-angle of LED	$\Phi_{\frac{1}{2}}$	60°
The vertical distance	d_h	2 m
The area of PD	A	10 ⁻⁴ m ²
The responsivity of PD	R_o	0.54 A/W
The covariance matrix of noise	\mathbf{R}_n	2.5 × 10 ⁻¹⁶ \mathbf{I}_N
The FoV of the receiver	Ψ_m	30°
The refraction index of air	n_0	1
The refraction index of optical filter	n_{eff}	2

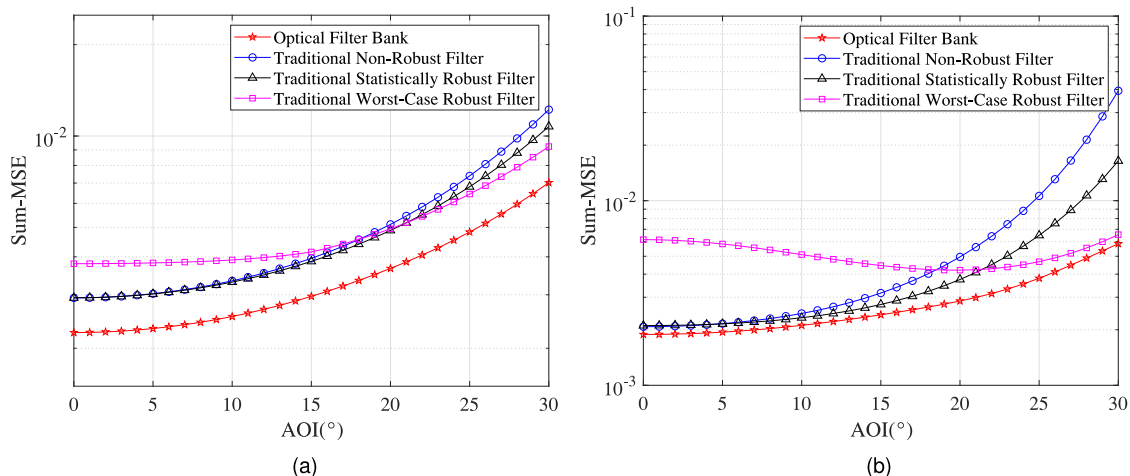


Fig. 8. Sum-MSE performance versus AOI for different optical filter designs. (a) RGB system. (b) RGBA system.

5.2 Performance Evaluation of Optical Filter Bank

In this subsection, we show the superiority of optical filter bank. To demonstrate that the proposed filtering structure are compatible for different configurations of LEDs, we consider both the RGB² and the RGBA system. For both RGB and RGBA systems, the optical filter bank with $N = 16$ and $\gamma = 0.5$ is used, and three benchmarks are based on traditional optical filter designs:

- Non-robust filter [18]: each optical filter corresponds to a monochromatic LED, and the optical filters are designed to minimize the sum-MSE at normal incidence.
- Statistically robust filter [18]: each optical filter corresponds to a monochromatic LED, and the optical filters are designed to minimize the average sum-MSE over all AOIs.
- Worst-case robust filter [18]: each optical filter corresponds to a monochromatic LED, and the optical filters are designed to minimize the sum-MSE at the worst-case AOI.

Fig. 8(a) and 8(b) illustrates the sum-MSE performance versus the AOI of the proposed optical filter bank and traditional optical filter designs in RGB and RGBA systems, respectively. One can see that in both RGB and RGBA systems, the proposed optical filter bank has significant performance improvement. The traditional non-robust filter achieves its minimum sum-MSE at normal incidence, while the sum-MSE degrades dramatically as the AOI increases. The traditional statistically and worst-case robust filters aim to achieve robust performance as the AOI varies, and they sacrifice the sum-MSE at normal incidence to improve the performance in the average and worst-case sense, respectively. Nevertheless, the proposed optical filter bank achieves lower and more robust sum-MSE than both of them.

Usually, traditional optical filters shall be specifically designed for RGB and RGBA transmitters. However, as illustrated in Fig. 8(a) and 8(b), the same optical filter bank with $N = 16$ and $\gamma = 0.5$ can achieve satisfactory performance for both RGB and RGBA systems, indicating its great compatibility for different transmitter configurations.

Furthermore, we compare the proposed transceiver design algorithm with traditional algorithms. In particular, in addition to the aforementioned algorithms in [29] and [30], the algorithm based on singular value decomposition (SVD) is also chosen as benchmarks [34], [42]. For the SVD-based algorithm, the right singular vectors of \mathbf{H} is chosen as the precoding matrix, and it is properly scaling within the constraints of MC-VLC as in (42). Still take the RGBA system using the optical filter bank with $N = 16$ and $\gamma = 0.5$ as an example.

²The RGB LEDs are implemented by the same QLED LZ4-00MA00 with the amber LED off. The brightness level is set to 150lm, and an equal-power ratio is adopted, leading to the white balance [41].

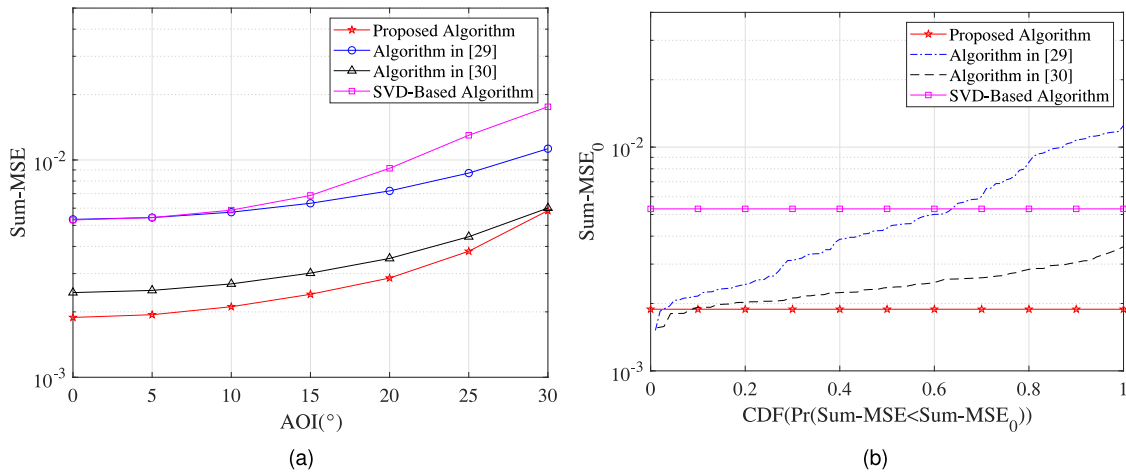


Fig. 9. (a) Sum-MSE performance versus AOI for different transceiver design algorithms in an RGBA system with the optical filter bank ($N = 16$ and $\gamma = 0.5$). (b) CDF of the final sum-MSE for the algorithms in [29] and [30] by generating 500 initial points in an RGBA system with the optical filter bank ($N = 16$ and $\gamma = 0.5$).

Considering that the algorithms in [29] and [30] depend on the initial points and it is hard to verify whether the initial point is proper or not in advance, we randomly generate 500 initial points and present the average performance at each AOI. Fig. 9(a) presents the sum-MSE performance versus AOI of different algorithms. One can see that the proposed algorithm achieves the best sum-MSE performance among them. The SVD-based algorithm achieves the worst performance, since it directly follows the transceiver design in RF communications but does not take the constraints in MC-VLC into account.

Fig. 9(b) illustrates the cumulative distribution function (CDF) of final sum-MSE for the algorithms in [29] and [30] by generating 500 initial points. The sum-MSE performances of the proposed algorithm and SVD-based algorithm are illustrated by constant lines, since they do not depend on the initial points. Obviously, the SVD-based algorithm has a poor sum-MSE performance, i.e., only 5×10^{-3} . The proposed algorithm achieves a stable and satisfactory sum-MSE close to 10^{-3} . For the algorithm in [29], about 95% of initial points lead to the sum-MSE worse than that of the proposed algorithm, and the worst initial point has a sum-MSE above 10^{-2} . For the algorithm in [30], about 90% of initial points lead to the sum-MSE worse than that of the proposed algorithm, and the worst initial point has a sum-MSE about 4×10^{-3} . Though there exist the initial points that also lead to the result close to 10^{-3} for the algorithms in [29] and [30], it usually costs plenty of computational complexity by searching a lot of initial points, as discussed in Section 4.4. While the proposed algorithm can easily achieve the sum-MSE performance close to the best of them with quite low complexity.

5.3 Characterization of Filtering Structure

Now, we would like to show the impact of N and γ on the performance of the optical filter bank. Fig. 10(a) illustrates the sum-MSE performance versus N with fixed $\gamma = 0.5$. As N increases, the sum-MSE first decreases and then increases. This result is consistent with the discussions in Remark 1. A small N leads to a large B_λ , where the cross-color interference is dominant; While a large N leads to a small B_λ , where the receiver noise is dominant.

Fig. 10(b) shows the sum-MSE performance versus γ with fixed $N = 16$. As γ increases, the sum-MSE first decreases and then increases. The reason is similar to the case about N .

Moreover, we would like to demonstrate the impact of the scaling operation of the proposed transceiver design algorithm, as discussed in Remarks 2 and 3.

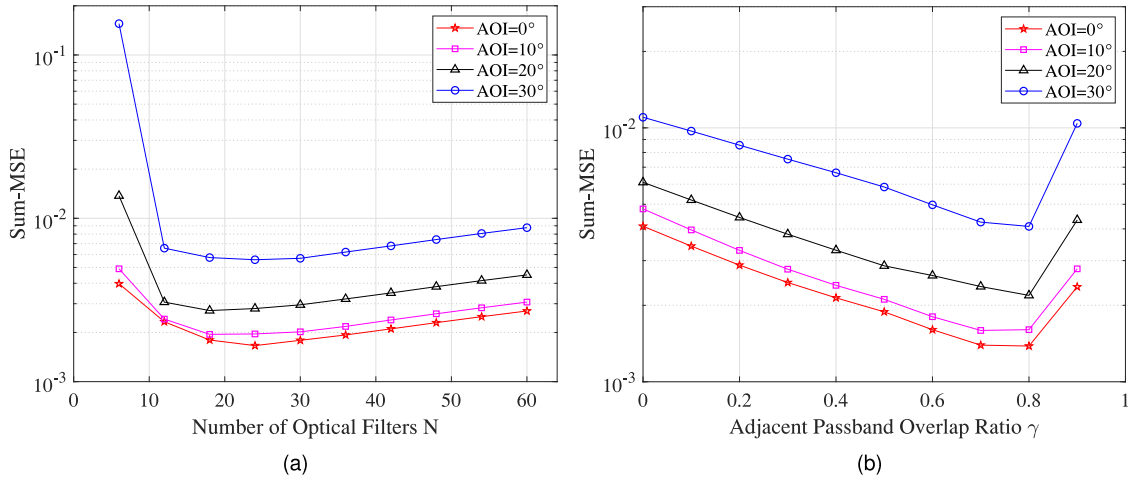


Fig. 10. (a) Sum-MSE performance versus N in an RGBA system ($\gamma = 0.5$). (b) Sum-MSE performance versus γ in an RGBA system ($N = 16$).

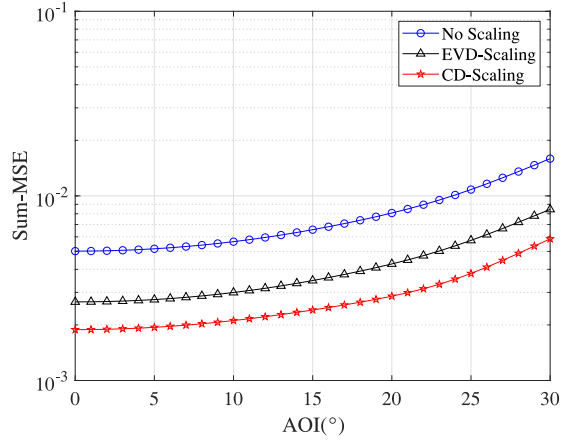


Fig. 11. Sum-MSE performance versus AOI for different scaling operations of the proposed algorithm in an RGBA system with the optical filter bank ($N = 16$ and $\gamma = 0.5$).

Fig. 11 shows the sum-MSE performance versus AOI for the proposed transceiver design algorithm with CD-scaling, EVD-scaling, and no scaling in an RGBA system using the optical filter bank with $N = 16$ and $\gamma = 0.5$. One can see that both the CD-scaling and EVD-scaling achieve lower sum-MSE than the case with no scaling. This result verifies the effectiveness of the scaling operation in (42). Besides, CD-scaling achieves a better performance than EVD-scaling.

To better understand why CD-scaling achieves a lower sum-MSE than EVD-scaling, we take $\text{AOI} = 0^\circ$ as an example and present the $\hat{\mathbf{W}}$ obtained by CD and EVD:

$$\hat{\mathbf{W}}^{(\text{CD})} = \begin{bmatrix} 0.1225 & 0 & 0 & 0 \\ -0.0293 & 0.1093 & 0 & 0 \\ 0.0012 & -0.0059 & 0.2172 & 0 \\ -0.0001 & 0.005 & -0.0098 & 0.1864 \end{bmatrix}, \quad (43)$$

$$\hat{\mathbf{W}}^{(\text{EVD})} = \begin{bmatrix} -0.0015 & 0.0002 & -0.1069 & 0.0598 \\ 0.0044 & -0.0005 & 0.0789 & 0.081 \\ -0.2151 & 0.0306 & 0.0023 & 0.0012 \\ 0.0359 & 0.1831 & -0.0002 & -0.0001 \end{bmatrix}. \quad (44)$$

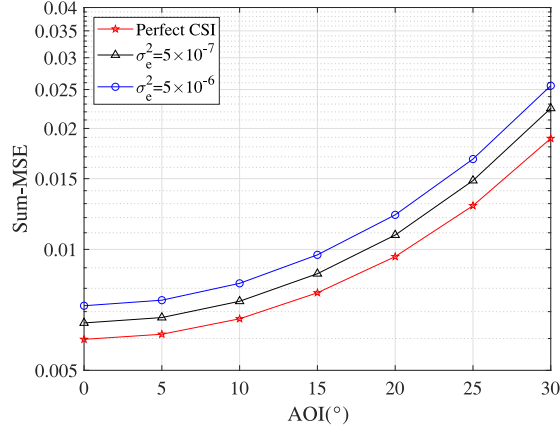


Fig. 12. Sum-MSE performance in the case with CSI error as the receiver moves.

Note that $\hat{\mathbf{W}}^{(\text{CD})}$ and $\hat{\mathbf{W}}^{(\text{EVD})}$ have same the Frobenius norm, i.e., $\|\hat{\mathbf{W}}^{(\text{CD})}\|_F = \|\hat{\mathbf{W}}^{(\text{EVD})}\|_F = 0.331$, since they are obtained by decomposing the same \mathbf{Q}^* . However, the l_1 norm vector of the rows of $\hat{\mathbf{W}}^{(\text{CD})}$ and $\hat{\mathbf{W}}^{(\text{EVD})}$ are $[0.1225, 0.1386, 0.2243, 0.1967]^T$ and $[0.1684, 0.1648, 0.2493, 0.2191]^T$, respectively. One can see that the l_1 norm of each row of $\hat{\mathbf{W}}^{(\text{CD})}$ is smaller than that of $\hat{\mathbf{W}}^{(\text{EVD})}$. Thus, $\hat{\mathbf{W}}^{(\text{CD})}$ can scale more largely than $\hat{\mathbf{W}}^{(\text{EVD})}$, i.e., $\xi_{\min}(\Lambda^{(\text{CD})}) = 1.632 > \xi_{\min}(\Lambda^{(\text{EVD})}) = 1.373$. That might be why CD-scaling leads to a lower sum-MSE than EVD-scaling.

To be more practical, Fig. 12 demonstrates the performance of the proposed transceiver design algorithm with the imperfect channel state information (CSI). The estimation error is assumed as Gaussian distribution with $\sigma_e^2 = 5 \times 10^{-7}$ and 5×10^{-6} , respectively. Compared with the perfect CSI case, the performance degrades slightly in the imperfect CSI case. It indicates that our proposed algorithm is insensitive to the CSI estimation error, and is still effective even if the receiver is moving fast and the channel information is outdated.

6. Conclusion

In this paper, we proposed a novel filtering structure named optical filter bank for MC-VLC to address the performance degradation issue caused by the CWL shift. We first established the channel model and signal model for the MC-VLC systems using optical filter bank. Then, we investigated the linear transceiver design including the precoding and the equalization, and proposed an effective algorithm with low complexity. The stability and superiority of the proposed transceiver using optical filter bank was verified by the simulation results at different AOIs.

Appendix

Proof of Theorem 1

By introducing an auxiliary matrix variable $\mathbf{T} \in \mathbb{R}^{N \times N}$, problem (38) has its equivalent form as

$$\min_{\mathbf{Q}, \mathbf{T}} \text{Tr}(\mathbf{T}\mathbf{R}_n) \quad (45a)$$

$$\text{s.t. } M[\mathbf{Q}]_{jj} \leq \min \left\{ \left(\frac{L_T c_j}{\eta_j} - x_{\text{on},j} \right)^2, \left(x_{\text{sat},j} - \frac{L_T c_j}{\eta_j} \right)^2 \right\} \quad (45b)$$

$$\mathbf{Q} \succeq \mathbf{0} \quad (45c)$$

$$\mathbf{T} \succeq (\sigma_s^2 \mathbf{H}\mathbf{Q}\mathbf{H}^T + \mathbf{R}_n)^{-1}. \quad (45d)$$

The equivalence between problems (45) and (38) can be easily explained. Since \mathbf{R}_n is positive semi-definite, we have $\text{Tr}(\mathbf{TR}_n) \geq \text{Tr}((\sigma_s^2 \mathbf{HQH}^T + \mathbf{R}_n)^{-1} \mathbf{R}_n)$ whenever $\mathbf{T} \succeq (\sigma_s^2 \mathbf{HQH}^T + \mathbf{R}_n)^{-1}$ [39]. Note that problem (45) aims to minimize $\text{Tr}(\mathbf{TR}_n)$. Thus, a monotonicity argument ensures that the equality $\mathbf{T} = (\sigma_s^2 \mathbf{HQH}^T + \mathbf{R}_n)^{-1}$ must hold at optimality for problem (45). Thus, problems (45) and (38) are equivalent.

Besides, the constraint $\mathbf{T} \succeq (\sigma_s^2 \mathbf{HQH}^T + \mathbf{R}_n)^{-1}$ can be rewritten via Schur's complement as the following linear matrix inequality (LMI) [36]:

$$\begin{bmatrix} \mathbf{T} & \mathbf{I} \\ \mathbf{I} & \sigma_s^2 \mathbf{HQH}^T + \mathbf{R}_n \end{bmatrix} \succeq \mathbf{0}. \quad (46)$$

Therefore, problem (45) has the equivalent formulation in (39). Since the objective function is linear and the constraints are either linear or positive semi-definite, problem (39) is an SDP problem. This completes the proof of Theorem 1.

References

- [1] P. Ge, X. Ling, J. Wang, X. Liang, R. Zhang, and C. Zhao, "Optical filter bank for multi-color visible light communications," in *Proc. IEEE Global Commun. Conf.*, 2019, pp. 1–6.
- [2] L. E. M. Matheus, A. B. Vieira, L. F. M. Vieira, M. A. M. Vieira, and O. Gnowali, "Visible light communication: Concepts, applications and challenges," *IEEE Commun. Surveys Tuts.*, vol. 21, no. 4, pp. 3204–3237, Oct.–Dec. 2019.
- [3] T. Komine and M. Nakagawa, "Fundamental analysis for visible light communication system using LED lights," *IEEE Trans. Consum. Electron.*, vol. 50, no. 1, pp. 100–107, Feb. 2004.
- [4] X. Ling, J. Wang, X. Liang, Z. Ding, C. Zhao, and X. Gao, "Biased multi-LED beamforming for multicarrier visible light communications," *IEEE J. Sel. Areas Commun.*, vol. 36, no. 1, pp. 106–120, Jan. 2018.
- [5] X. Ling, S. Li, P. Ge, J. Wang, N. Chi, and X. Gao, "Optimal DCO-OFDM signal shaping with double-sided clipping in visible light communications," *Opt. Exp.*, vol. 28, no. 21, pp. 30 391–30 409, Oct. 2020.
- [6] J. Chen, Z. Wang, and R. Jiang, "Downlink interference management in cell-free VLC network," *IEEE Trans. Veh. Technol.*, vol. 68, no. 9, pp. 9007–9017, Sep. 2019.
- [7] D. Karunatilaka, F. Zafar, V. Kalavally, and R. Parthiban, "LED based indoor visible light communications: State of the art," *IEEE Commun. Surveys Tuts.*, vol. 17, no. 3, pp. 1649–1678, Jul.–Sep. 2015.
- [8] R. Jiang, Z. Wang, Q. Wang, and L. Dai, "Multi-user sum-rate optimization for visible light communications with lighting constraints," *J. Lightw. Technol.*, vol. 34, no. 16, pp. 3943–3952, Aug. 2016.
- [9] C. Gong, S. Li, Q. Gao, and Z. Xu, "Power and rate optimization for visible light communication system with lighting constraints," *IEEE Trans. Signal Process.*, vol. 63, no. 16, pp. 4245–4256, Aug. 2015.
- [10] Y. Wang, L. Tao, X. Huang, J. Shi, and N. Chi, "8-Gb/s RGBY LED-Based WDM VLC system employing high-order CAP modulation and hybrid post equalizer," *IEEE Photon. J.*, vol. 7, no. 6, pp. 1–7, Dec. 2015.
- [11] H. Chun *et al.*, "LED based wavelength division multiplexed 10 gb/s visible light communications," *J. Lightw. Technol.*, vol. 34, no. 13, pp. 3047–3052, Jul. 2016.
- [12] L. Cui, Y. Tang, H. Jia, J. Luo, and B. Gnade, "Analysis of the multichannel WDM-VLC communication system," *J. Lightw. Technol.*, vol. 34, no. 24, pp. 5627–5634, Dec. 2016.
- [13] S. Chen and C. Chow, "Color-shift keying and code-division multiple-access transmission for RGB-LED visible light communications using mobile phone camera," *IEEE Photon. J.*, vol. 6, no. 6, Dec. 2014, Art. no. 7904106.
- [14] Semrock Inc., "Semrock optical filter product families," 2019. Accessed: Jan. 1, 2019. [Online]. Available: <https://www.semrock.com/product-families.aspx>
- [15] K. Liang, C.-W. Chow, and Y. Liu, "RGB visible light communication using mobile-phone camera and multi-input multi-output," *Opt. Exp.*, vol. 24, no. 9, pp. 9383–9388, May. 2016.
- [16] S.-H. Chen and C.-W. Chow, "Color-filter-free spatial visible light communication using RGB-LED and mobile-phone camera," *Opt. Exp.*, vol. 22, no. 25, pp. 30 713–30 718, Dec. 2014.
- [17] P. Ge, X. Liang, J. Wang, and C. Zhao, "Optical filters design for multi-color visible light communications," in *Proc. IEEE Global Commun. Conf.*, 2017, pp. 1–7.
- [18] P. Ge, X. Liang, J. Wang, C. Zhao, X. Gao, and Z. Ding, "Optical filter designs for multi-color visible light communication," *IEEE Trans. Commun.*, vol. 67, no. 3, pp. 2173–2187, Mar. 2019.
- [19] Semrock Inc., "Semrock optical filters catalogue," 2019. Accessed: Mar. 1, 2019. [Online]. Available: <https://www.semrock.com/Data/Sites/1/semrockpdfs/SemrockCatalog-2019.pdf>
- [20] J. Sticklus, M. Hieronymi, and P. A. Hoehner, "Effects and constraints of optical filtering on ambient light suppression in LED-based underwater communications," *Sensors*, vol. 18, no. 11, pp. 1–21, Oct. 2018.
- [21] N. Uehara, R. Okuda, T. Shidara, and R. Otowa, "Advanced thin-film filter for passive optical networks," in *Proc. Tech. Dig., Opt. Fiber Commun. Conf.*, 2005, pp. 1–3.
- [22] Y. Ren, Y. Guo, P. Xing, J. Huo, and S. Zhang, "Investigation on the wavelength division multiplexing optical thin-film filter," in *Proc. Wireless Opt. Commun. Conf.*, 2010, pp. 1–4.
- [23] P. Yeh, *Optical Waves in Layered Media*. New York, NY, USA: Wiley, 1988.
- [24] G. He and L. Zheng, "A model for LED spectra at different drive currents," *Chin. Opt. Lett.*, vol. 8, no. 11, pp. 1090–1094, Nov. 2010.

- [25] T. Xiao, C. Gong, Q. Gao, and Z. Xu, "Channel characterization for multi-color VLC for feedback and beamforming design," in *Proc. IEEE Int. Conf. Commun. Workshops*, 2018, pp. 1–6.
- [26] T. E. Bitencourt Cunha, J. M. G. Linnartz, and X. Deng, "Throughput of optical WDM with wide LED spectra and imperfect color-detecting filters," in *Proc. Wireless Opt. Commun. Conf.*, 2020, pp. 1–6.
- [27] L. C. Mathias, A. R. C. e Souza, and T. A. ao, "Wavelength widths of optical filters for optimum SINR in WDM-VLC systems," *Appl. Opt.*, vol. 59, no. 18, pp. 5615–5624, Jun. 2020.
- [28] X. Ling, J. Wang, X. Liang, Z. Ding, and C. Zhao, "Offset and power optimization for DCO-OFDM in visible light communication systems," *IEEE Trans. Signal Process.*, vol. 64, no. 2, pp. 349–363, Jan. 2016.
- [29] K. Ying, H. Qian, R. J. Baxley, and S. Yao, "Joint optimization of precoder and equalizer in MIMO VLC systems," *IEEE J. Sel. Areas Commun.*, vol. 33, no. 9, pp. 1949–1958, Sep. 2015.
- [30] B. Li, R. Zhang, W. Xu, C. Zhao, and L. Hanzo, "Joint dimming control and transceiver design for MIMO-aided visible light communication," *IEEE Commun. Lett.*, vol. 20, no. 11, pp. 2193–2196, Nov. 2016.
- [31] J. Dong, Y. Zhu, Y. Zhang, and Z. Sun, "Illumination-adapted transceiver design for quadrichromatic light-emitting diode based visible light communication," *IEEE Photon. J.*, vol. 10, no. 3, Jun. 2018, Art. no. 7904010.
- [32] R. Wang *et al.*, "Linear transceiver designs for MIMO indoor visible light communications under lighting constraints," *IEEE Trans. Commun.*, vol. 65, no. 6, pp. 2494–2508, Jun. 2017.
- [33] N. Huang, X. Wang, and M. Chen, "Transceiver design for MIMO VLC systems with integer-forcing receivers," *IEEE J. Sel. Areas Commun.*, vol. 36, no. 1, pp. 66–77, Jan. 2018.
- [34] K. Ying, H. Qian, R. J. Baxley, and G. T. Zhou, "MIMO transceiver design in dynamic-range-limited VLC systems," *IEEE Photon. Technol. Lett.*, vol. 28, no. 22, pp. 2593–2596, Nov. 2016.
- [35] X. Liang, M. Yuan, J. Wang, Z. Ding, M. Jiang, and C. Zhao, "Constellation design enhancement for color-shift keying modulation of quadrichromatic LEDs in visible light communication," *J. Lightw. Technol.*, vol. 35, no. 17, pp. 3650–3663, Sep. 2017.
- [36] C. R. J. Roger A. Horn, *Matrix Analysis*. New York, NY, USA: Cambridge Univ. Press, 1990.
- [37] T. V. Pham, H. Le-Minh, and A. T. Pham, "Multi-user visible light communication broadcast channels with zero-forcing precoding," *IEEE Trans. Commun.*, vol. 65, no. 6, pp. 2509–2521, Jun. 2017.
- [38] S. Boyd and L. Vandenberghe, *Convex Optimization*. New York, NY, USA: Cambridge Univ. Press, 2004.
- [39] Z. -Q. Luo, T. N. Davidson, G. B. Giannakis, and K. M. Wong, "Transceiver optimization for block-based multiple access through ISI channels," *IEEE Trans. Signal Process.*, vol. 52, no. 4, pp. 1037–1052, Apr. 2004.
- [40] B. Fahs, M. Romanowicz, and M. M. Hella, "A Gbps building-to-building VLC link using standard CMOS avalanche photodiodes," *IEEE Photon. J.*, vol. 9, no. 6, Dec. 2017.
- [41] Q. Gao, R. Wang, Z. Xu, and Y. Hua, "Power-efficient high-dimensional constellation design for visible light communications," in *Proc. Opto-Electron. Commun. Conf.*, 2015, pp. 1–3.
- [42] F. Yang, J. -B. Wang, M. Cheng, J. -Y. Wang, M. Lin, and J. Cheng, "A partially dynamic subarrays structure for wideband mmWave MIMO systems," *IEEE Trans. Commun.*, vol. 68, no. 12, pp. 7578–7592, Dec. 2020.